

## Discovery of A Low-mass Strong-lens System in SMACS J0723.3-7327

LIMENG DENG,<sup>1,2</sup> YIPING SHU,<sup>1</sup> LEI WANG,<sup>1</sup> GUOLIANG LI,<sup>1</sup> GABRIEL BARTOSCH CAMINHA,<sup>3</sup> JIANG DONG,<sup>1,2</sup> ZIZHAO HE,<sup>1</sup>  
HAN QU,<sup>1,2</sup> AND RUIBIAO LUO<sup>1</sup>

<sup>1</sup>*Purple Mountain Observatory, Chinese Academy of Sciences, Nanjing, Jiangsu 210028, China*

<sup>2</sup>*School of Astronomy and Space Sciences, University of Science and Technology of China, Hefei 230026, China*

<sup>3</sup>*Technische Universität München, Physik-Department, James-Frank Str. 1, 85748 Garching, Germany*

### ABSTRACT

We report the discovery of an intriguing, low-mass galaxy-scale strong-lens system in the SMACS J0723.3-7327 galaxy cluster. By modeling James Webb Space Telescope imaging and Very Large Telescope Multi-Unit Spectroscopic Explorer spectroscopic data, we find that the lens is cluster member galaxy at  $z = 0.397$  with an Einstein radius of  $0''.424 \pm 0''.012$ , stellar mass of  $M_* = (3.3 \pm 0.8) \times 10^{10} M_\odot$ , half-light radius of  $\sim 1$  kpc, and central stellar velocity dispersion of  $140 \pm 6$  km s<sup>-1</sup>. This lens galaxy is one of the few strong lens galaxies known to date that have stellar mass as low as  $M_* \sim 10^{10.5} M_\odot$ , offering an exceptional opportunity to peek into the population of low-mass galaxies that has largely remained unexplored in the context of strong-lensing studies. This strong lens system can also assist in assessing the systematic uncertainty in the lens modeling of cluster member galaxies.

*Keywords:* Strong gravitational lensing (1643) — Galaxy formation (595) — Galaxy evolution (594)

### 1. INTRODUCTION

Strong gravitational lensing is the phenomenon of forming multiple images of a background source object by the gravity of a foreground lens object. In particular, galaxy-scale strong-lens systems, where the lens objects are galaxies, are powerful tools for understanding galaxy formation and evolution. For example, it has been suggested that the lens galaxies studied generally prefer a Salpeter initial mass function (IMF) (e.g., Spiniello et al. 2011; Oguri et al. 2014) and their dark-matter fractions increase with stellar mass and velocity dispersion (e.g., Auger et al. 2010; Shu et al. 2015; Shajib et al. 2021). Correlations between the central mass density profile of lens galaxies and galaxy properties such as stellar mass density, stellar mass, and redshift have been characterized (e.g., Auger et al. 2010; Bolton et al. 2012; Sonnenfeld et al. 2013; Shu et al. 2015; Li et al. 2018), providing constraints on the impact of baryonic physics and mergers (e.g., Nipoti et al. 2009; Velliscig et al. 2014; Sonnenfeld et al. 2014). By measuring the shape and

alignment of the dark matter distribution and stellar mass distribution, studies have shown that dark-matter halos of those lens galaxies are typically rounder than the stellar mass distributions and the misalignment angles between dark matter and stars are generally small (e.g., Koopmans et al. 2006; Bruderer et al. 2016; Shu et al. 2016).

Nevertheless, such knowledge have been largely limited to massive galaxies because lens galaxies in currently known strong-lens samples typically have stellar mass of  $10^{11}$ – $10^{12} M_\odot$ . On the other hand, stellar dynamical analyses of nearby galaxies ( $z \lesssim 0.1$ ) suggest that the dark-matter fraction reaches a minimum at a characteristic stellar mass of  $M_* \sim 3 \times 10^{10} M_\odot$  and increases towards both low- and high-mass ends (e.g., Cappellari et al. 2013a). The IMF is also found to vary with velocity dispersion in the sense that galaxies with lower velocity dispersions tend to have lighter IMF (e.g. Chabrier or Kroupa, Cappellari et al. 2013b; Li et al. 2017). Low-mass lens galaxies ( $M_* \lesssim 10^{10.5} M_\odot$ ) can hence provide highly complementary constraints, especially at high redshifts where spatially-resolved stellar kinematics observations remain challenging.

A key obstacle in discovering low-mass lenses is the need for high angular resolution data. For typical lens



**Figure 1.** Color composite image of SMACS J0723 generated from JWST NIRCcam data in six filters (F090W, F150W, F200W, F277W, F356W, F444W). The inset figure provides an enlarged view of the strong-lens system studied in this work.

and source redshifts of 0.5 and 1.5, the angular separations between multiple lensed images are on the order of  $2''$  when the lensing mass is  $10^{11.5} M_{\odot}$ , which can be easily resolved in existing imaging data from wide-field surveys such as the Sloan Digital Sky Survey, Dark Energy Survey, Legacy Surveys, etc. When the lensing mass becomes  $10^{10.5} M_{\odot}$ , the angular separations decrease to  $\approx 0''.7$ , significantly hindering the detectability.

In this work, we will report a serendipitous discovery of a low-mass ( $M_* \approx 10^{10.5} M_{\odot}$ ) strong-lens system from James Webb Space Telescope (JWST) observations of the SMACS J0723.3-7327 galaxy cluster (hereafter SMACS J0723). This paper is organized as follows. We describe the imaging and spectroscopic data in Section 2, and present the strong lens modeling procedures and results in Section 3. Discussions and conclusions are provided in Section 4 and Section 5. All magnitudes are on the AB scale, and a standard concordance cosmology with  $\Omega_m = 0.3$ ,  $\Omega_{\Lambda} = 0.7$ , and  $h = 70 \text{ km s}^{-1} \text{ Mpc}^{-1}$  is assumed.

## 2. DATA

### 2.1. JWST imaging data

The JWST Early Release Observations (ERO) of the SMACS J0723 galaxy cluster include broadband imaging by the NIRCcam and MIRI as well as multi-object and slitless spectroscopy by the NIRSpec and NIRSS (Programme ID: 2736, Pontoppidan et al. 2022). In this work, we focused on the NIRCcam imaging data in six

filters covering the wavelength range from roughly  $0.8 \mu\text{m}$  to  $5.0 \mu\text{m}$ , i.e. F090W, F150W, F200W, F277W, F356W, and F444W. In each NIRCcam filter, observations were split into nine sub-exposures (following the INTRAMODULEX dither pattern) with a total exposure time of  $\approx 7537$  seconds. Regarding data reduction, we made use of the UPdec-Webb dataset constructed by Wang et al. (2025), who reduced and coadded the NIRCcam imaging data of SMACS J0723 using a customized algorithm — Up-sampling and PSF Deconvolution Coaddition (UPDC, Wang et al. 2022). As demonstrated in Wang et al. (2025), the UPdec-Webb images exhibit significant improvement in terms of photometry accuracy and faint source detectability compared to coadded images processed by the standard Drizzle algorithm. The UPdec-Webb dataset<sup>1</sup> contains 11 imaging files per filter, which correspond to a directly coadded image (iter0) and 10 deconvolved images produced after different iterations of PSF deconvolution (iter1-iter10). In this work, we used the UPdec-Webb coadded images, which are supersampled by a factor of two, resulting a pixel scale of  $0''.0155/\text{pixel}$  in F090W, F150W, and F200W and  $0''.031/\text{pixel}$  in F277W, F356W, and F444W.

A color composite image of the central region of SMACS J0723 constructed from the UPdec-Webb coadded images in all six NIRCcam filters is presented in Fig-

<sup>1</sup> Available at the National Astronomical Data Center: doi:10.12149/101436.

ure 1. The galaxy-scale strong-lens system we discovered and analyzed in this work, denoted as SMACS J0723-SL, is located at R.A. =  $110^{\circ}.8488458$ , Decl. =  $-73^{\circ}.4606771$ , about 31.3 arcsecs ( $\approx 167$  kpc) southeast from the brightest cluster galaxy (BCG). In this system, we clearly see an orange-ish question-mark structure surrounding the central galaxy, indicative of a strong lensing effect. The radius of the structure is about  $0''8$ .

## 2.2. MUSE data cube

The SMACS J0723 cluster was also observed by the Multi-Unit Spectroscopic Explorer (MUSE) integral field spectrograph in 2019 under Programme ID: 0102.A-0718 (PI: A. Edge). In this work, we used the reduced data cube from [Caminha et al. \(2022\)](#), which has a 1 arcmin<sup>2</sup> field of view centered on the BCG and covers the wavelength range 4750Å–9350Å. The spectral resolution is  $\approx 2.4\text{Å}$  with a sampling of 1.25Å per spectral pixel. According to the redshift catalog built from the MUSE data cube by [Caminha et al. \(2022\)](#), the lens galaxy in SMACS J0723-SL has a spectroscopic redshift of 0.3970, confirming it as a cluster member galaxy. In addition, the bright tail of the question-mark structure was also cataloged in [Caminha et al. \(2022\)](#) with a spectroscopic redshift of 1.4792. The two different redshifts further support the strong lensing interpretation.

## 3. STRONG LENS MODELING

Encouraged by the imaging and spectroscopic evidence, we aim to obtain a sensible strong lens model for SMACS J0723-SL to firmly establish its strong lensing nature. Although strong-lens models of the SMACS J0723 cluster have been constructed by several teams (e.g., [Caminha et al. 2022](#); [Golubchik et al. 2022](#); [Sharon et al. 2023](#); [Mahler et al. 2023](#)), the lens galaxy in SMACS J0723-SL was either completely ignored or modeled simultaneously with all other member galaxies following a scaling relation, without using any constraint from the potential lensing features around it. In this work, we explicitly model the lens galaxy in SMACS J0723-SL.

### 3.1. Model set-up

For the lens galaxy in SMACS J0723-SL, we used an elliptical power law (EPL) profile to model its projected total-mass distribution, which is parameterized as:

$$\Sigma(x, y) = \Sigma_{\text{crit}} \frac{3 - \gamma_{\text{EPL}}}{2} \left( \frac{\theta_{\text{E}}}{\sqrt{qx^2 + y^2/q}} \right)^{\gamma_{\text{EPL}} - 1}, \quad (1)$$

where  $\theta_{\text{E}}$  is the Einstein radius,  $\gamma_{\text{EPL}}$  is the power-law slope,  $q$  is the minor-to-major axis ratio,  $x$  and  $y$  are

defined in a coordinate system aligned with the major and minor axis of the lens mass distribution.  $\Sigma_{\text{crit}}$  is the critical density defined as  $\Sigma_{\text{crit}} = \frac{c^2}{4\pi G} \frac{D_S}{D_L D_{LS}}$ , where  $D_L$ ,  $D_S$ , and  $D_{LS}$  are angular diameter distances of the lens, the source, and from the lens to the source respectively.

To account for the contribution from the cluster to the lensing potential, we utilized the lens model of SMACS J0723 constructed using the JWST ERO data by [Caminha et al. \(2022, hereafter C22\)](#), or more specifically, their convergence and shear maps (100 each, corresponding to 100 Monte Carlo realizations). In principle, we should directly adopt C22 results as the external convergence and external shear in our model. However, only the shear strength map was available in C22 but not the shear position angle. We thus had to optimize for the external shear, the lensing potential of which is parameterized as

$$\psi_{\text{shear}} = -\frac{1}{2} \gamma_{\text{shear}} (x^2 + y^2) \cos 2(\phi - \phi_{\text{shear}}), \quad (2)$$

where  $\gamma_{\text{shear}}$  and  $\phi_{\text{shear}}$  are the strength and position angle of the external shear.

Regarding the external convergence, we selected a  $5'' \times 5''$  region centered on SMACS J0723-SL from the C22 convergence maps. We found that the mean convergence in this region is  $\sim 0.4$  and the spatial variation is  $\sim 0.017$ . We therefore assumed the external convergence can be approximated as a constant  $\kappa_{\text{ext}}$ , i.e. a mass sheet. We computed the mean convergence in the selected region for each realization and adopted the median and standard deviation of the 100 mean convergence, 0.40 and 0.018, as the median and  $1\sigma$  uncertainty for  $\kappa_{\text{ext}}$ . In our modeling process, we then fixed  $\kappa_{\text{ext}}$  to 0.40. To account for the impact of the  $\kappa_{\text{ext}}$  uncertainty on the other lens parameters, we actually made use of the mass-sheet degeneracy (MSD, [Falco et al. 1985](#); [Schneider & Sluse 2013](#); [Khadka et al. 2024](#)). According to the MSD, the following two sets of lensing potentials give identical lensed imaging signals,

$$\kappa'(x, y) = \lambda \kappa(x, y) + (1 - \lambda), \quad (3)$$

when the source plane coordinate is also rescaled as  $\vec{\beta} = \lambda \vec{\beta}$ . Therefore,  $\theta_{\text{E}}$  and  $\gamma_{\text{shear}}$  will change with  $\kappa_{\text{ext}}$  as

$$\frac{\delta \theta_{\text{E}}}{\theta_{\text{E}}} = \frac{\delta \kappa_{\text{ext}}}{(\gamma_{\text{EPL}} - 1)(1 - \kappa_{\text{ext}})}, \quad (4)$$

$$\frac{\delta \gamma_{\text{shear}}}{\gamma_{\text{shear}}} = \frac{\delta \kappa_{\text{ext}}}{1 - \kappa_{\text{ext}}}. \quad (5)$$

We used the Sérsic profile ([Sérsic 1963](#)) to model the light distributions of the lens galaxy and source galaxy. The number of Sérsic components was determined by

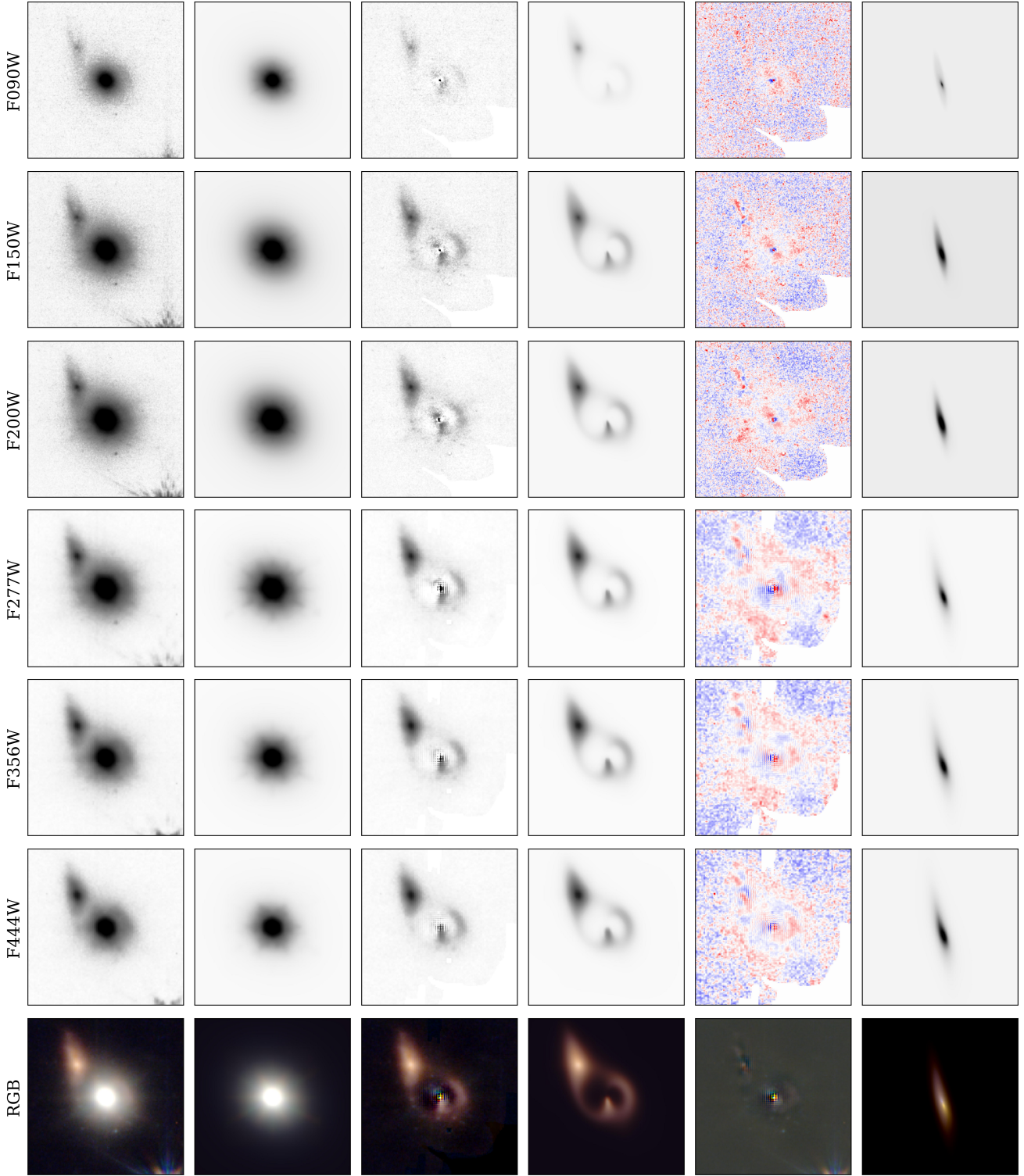


**Figure 2.** Best-fitting results. Within each row, from left to right, we show the data, lens light model, lens light-subtracted data, lensed image model, normalized residual, and source light model. The first six rows correspond to the six filters and the last row is a color composite equivalent generated by combining the six filters.

the data. In each filter, we found that a single Sérsic was sufficient for the lens galaxy while two were needed for the source galaxy, which appears to have a relatively

compact component and an extended component. The point spread function (PSF) models were derived from

**Table 1.** Lens model parameters (median and the 68% confidence interval).

$\theta_E$ (")	$\gamma_{\text{EPL}}$	$\phi_{\text{EPL}}$ (°)	$q_{\text{EPL}}$	$\gamma_{\text{shear}}$	$\phi_{\text{shear}}$ (°)
$0.424^{+0.012}_{-0.012}$	$2.10^{+0.03}_{-0.07}$	$-60.4^{+1.8}_{-5}$	$0.87^{+0.05}_{-0.04}$	$0.152^{+0.018}_{-0.022}$	$-20.7^{+0.7}_{-0.5}$

**Table 2.** Lens light parameters (median and the 68% confidence interval). Column 2 is the integrated magnitude. Columns 3–4 are the  $x$  and  $y$  coordinates of the Sérsic component relative to the cutout center. Columns 5–8 correspond to the position angle of the major axis (east from north), minor-to-major axis ratio, half-light radius, and Sérsic index.

Filter	$m_{AB}$	$\Delta x$ (")	$\Delta y$ (")	$\phi$ (°)	$q$	$R_e$ (")	$n$
F090W	$20.8526^{+0.0017}_{-0.0022}$	$0.00405^{+0.00006}_{-0.00007}$	$-0.01018^{+0.00010}_{-0.00021}$	$-42.19^{+0.18}_{-0.26}$	$0.8746^{+0.0014}_{-0.0020}$	$0.2604^{+0.0011}_{-0.0010}$	$4.948^{+0.011}_{-0.015}$
F150W	$19.9180^{+0.003}_{-0.0014}$	$0.00405^{+0.00006}_{-0.00007}$	$-0.01018^{+0.00010}_{-0.00021}$	$-42.19^{+0.18}_{-0.26}$	$0.8746^{+0.0014}_{-0.0020}$	$0.2540^{+0.0008}_{-0.0012}$	$4.616^{+0.013}_{-0.04}$
F200W	$19.6748^{+0.0008}_{-0.0007}$	$0.00405^{+0.00006}_{-0.00007}$	$-0.01018^{+0.00010}_{-0.00021}$	$-42.19^{+0.18}_{-0.26}$	$0.8746^{+0.0014}_{-0.0020}$	$0.2498^{+0.0009}_{-0.0006}$	$4.496^{+0.03}_{-0.028}$
F277W	$19.7811^{+0.0024}_{-0.003}$	$0.00405^{+0.00006}_{-0.00007}$	$-0.01018^{+0.00010}_{-0.00021}$	$-42.19^{+0.18}_{-0.26}$	$0.8746^{+0.0014}_{-0.0020}$	$0.1998^{+0.0006}_{-0.0006}$	$4.428^{+0.029}_{-0.04}$
F356W	$20.2936^{+0.003}_{-0.0022}$	$0.00405^{+0.00006}_{-0.00007}$	$-0.01018^{+0.00010}_{-0.00021}$	$-42.19^{+0.18}_{-0.26}$	$0.8746^{+0.0014}_{-0.0020}$	$0.2072^{+0.0010}_{-0.0010}$	$3.896^{+0.023}_{-0.017}$
F444W	$20.587^{+0.006}_{-0.006}$	$0.00405^{+0.00006}_{-0.00007}$	$-0.01018^{+0.00010}_{-0.00021}$	$-42.19^{+0.18}_{-0.26}$	$0.8746^{+0.0014}_{-0.0020}$	$0.1935^{+0.0022}_{-0.0024}$	$3.587^{+0.016}_{-0.011}$

**Table 3.** Source light parameters (median and the 68% confidence interval). The columns are arranged in the same order as Table 2.

Filter	$m_{AB}$	$\Delta x$ (")	$\Delta y$ (")	$\phi$ (°)	$q$	$R_e$ (")	$n$	$\mu$
<b>Component 1</b>								
F090W	$26.919^{+0.06}_{-0.029}$	$-0.087^{+0.014}_{-0.010}$	$0.368^{+0.016}_{-0.021}$	$-75.8^{+2.6}_{-2.4}$	$0.331^{+0.005}_{-0.007}$	$0.102^{+0.003}_{-0.003}$	$1.495^{+0.04}_{-0.015}$	7.8
F150W	$25.36^{+0.06}_{-0.04}$	$-0.087^{+0.014}_{-0.010}$	$0.368^{+0.016}_{-0.021}$	$-75.8^{+2.6}_{-2.4}$	$0.331^{+0.005}_{-0.007}$	$0.1230^{+0.0016}_{-0.0019}$	$1.800^{+0.007}_{-0.009}$	8.1
F200W	$25.12^{+0.09}_{-0.05}$	$-0.087^{+0.014}_{-0.010}$	$0.368^{+0.016}_{-0.021}$	$-75.8^{+2.6}_{-2.4}$	$0.331^{+0.005}_{-0.007}$	$0.1143^{+0.0019}_{-0.004}$	$1.548^{+0.04}_{-0.009}$	8.0
F277W	$24.86^{+0.10}_{-0.04}$	$-0.087^{+0.014}_{-0.010}$	$0.368^{+0.016}_{-0.021}$	$-75.8^{+2.6}_{-2.4}$	$0.331^{+0.005}_{-0.007}$	$0.0997^{+0.0021}_{-0.005}$	$1.692^{+0.062}_{-0.024}$	7.7
F356W	$24.76^{+0.08}_{-0.05}$	$-0.087^{+0.014}_{-0.010}$	$0.368^{+0.016}_{-0.021}$	$-75.8^{+2.6}_{-2.4}$	$0.331^{+0.005}_{-0.007}$	$0.093^{+0.003}_{-0.004}$	$1.620^{+0.007}_{-0.008}$	7.7
F444W	$24.71^{+0.06}_{-0.03}$	$-0.087^{+0.014}_{-0.010}$	$0.368^{+0.016}_{-0.021}$	$-75.8^{+2.6}_{-2.4}$	$0.331^{+0.005}_{-0.007}$	$0.0940^{+0.0022}_{-0.0020}$	$1.656^{+0.06}_{-0.027}$	7.7
<b>Component 2</b>								
F090W	$27.05^{+0.05}_{-0.03}$	$-0.121^{+0.014}_{-0.012}$	$0.453^{+0.008}_{-0.017}$	$-82.4^{+2.2}_{-2.0}$	$0.158^{+0.006}_{-0.006}$	$0.133^{+0.005}_{-0.007}$	$0.194^{+0.006}_{-0.008}$	8.6
F150W	$25.757^{+0.04}_{-0.027}$	$-0.121^{+0.014}_{-0.012}$	$0.453^{+0.008}_{-0.017}$	$-82.4^{+2.2}_{-2.0}$	$0.158^{+0.006}_{-0.006}$	$0.1490^{+0.0024}_{-0.0022}$	$0.270^{+0.016}_{-0.016}$	8.6
F200W	$25.634^{+0.026}_{-0.021}$	$-0.121^{+0.014}_{-0.012}$	$0.453^{+0.008}_{-0.017}$	$-82.4^{+2.2}_{-2.0}$	$0.158^{+0.006}_{-0.006}$	$0.147^{+0.005}_{-0.004}$	$0.409^{+0.03}_{-0.018}$	8.2
F277W	$25.229^{+0.026}_{-0.022}$	$-0.121^{+0.014}_{-0.012}$	$0.453^{+0.008}_{-0.017}$	$-82.4^{+2.2}_{-2.0}$	$0.158^{+0.006}_{-0.006}$	$0.1425^{+0.0024}_{-0.003}$	$0.591^{+0.04}_{-0.016}$	8.0
F356W	$25.045^{+0.03}_{-0.022}$	$-0.121^{+0.014}_{-0.012}$	$0.453^{+0.008}_{-0.017}$	$-82.4^{+2.2}_{-2.0}$	$0.158^{+0.006}_{-0.006}$	$0.1381^{+0.0028}_{-0.0027}$	$0.640^{+0.04}_{-0.015}$	7.8
F444W	$24.957^{+0.05}_{-0.029}$	$-0.121^{+0.014}_{-0.012}$	$0.453^{+0.008}_{-0.017}$	$-82.4^{+2.2}_{-2.0}$	$0.158^{+0.006}_{-0.006}$	$0.1277^{+0.0028}_{-0.003}$	$0.756^{+0.016}_{-0.019}$	7.6

the (unsaturated) star closest to the lensing system using the method developed by Nie et al. (2023).

We simultaneously modeled the imaging data from all six filters. For the three shorter wavelength filters (i.e. F090W, F150W, and F200W), cutouts of  $325 \times 325$  pixels centered on SMACS J0723-SL were used, while cutouts of  $163 \times 163$  pixels were used for the three longer wavelength filters (i.e. F277W, F356W, and F444W). Each cutout is therefore roughly  $5''$  across. In the modeling process, we assumed that the lens light distributions in the six filters have the same center, axis ratio, and position angle. For the source galaxy, each of the two Sérsic models also has the same center, axis ratio, and posi-

tion angle across the six filters. We further fixed the lens mass center to the lens light center. In total, our model contained 54 non-linear parameters that need to be constrained, including 4 from the EPL model, 2 from the external shear model, 16 from the lens light models, and 32 from the source light models. The parameter inference was done using the open-source package *lenstronomy* (Birrer & Amara 2018).

### 3.2. Modeling results

Our modeling results are presented in Figure 2 and Tables 1, 2, 3. It can be seen that our model successfully reproduced the imaging data, especially the question-

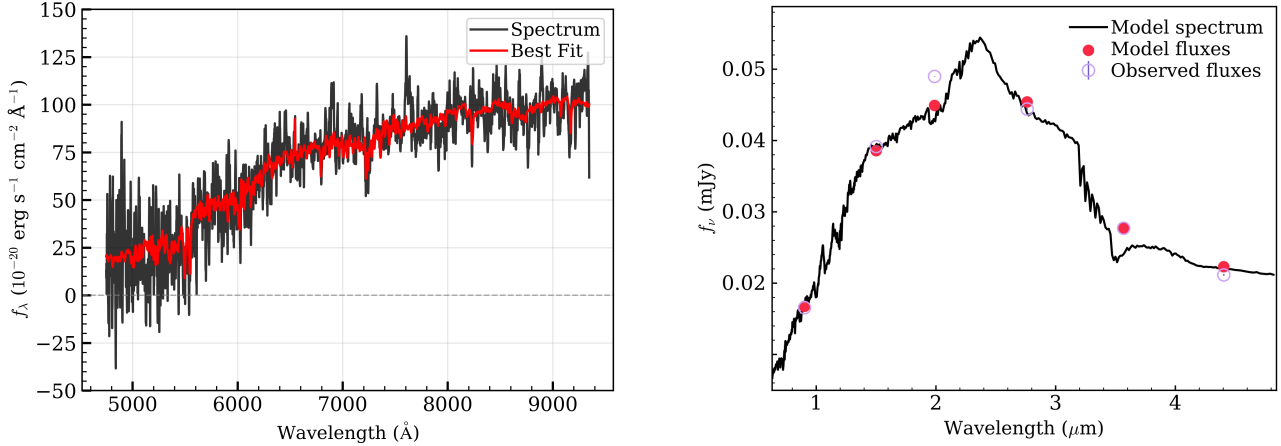


**Figure 3.** *Left:* pPXF velocity dispersion fitting result. The black line corresponds to the observed spectrum (smoothed for illustration purposes) and the red line corresponds to the best fit. *Right:* CIGALE SED fitting result. Open and filled circles correspond to the observed and model-predicted photometry.

mark structures. The reduced  $\chi^2$  value is 0.9976. The lens mass distribution is slight steeper than isothermal (i.e.  $\gamma = 2$ ), and is well aligned with its light distribution in terms of both the axis ratio and position angle. We thus confirmed that SMACS J0723-SL is a genuine strong-lens system. Furthermore, we found that the lens galaxy has an exceptionally small Einstein radius of  $0''.424 \pm 0''.012$ . We note that this Einstein radius is what the lens galaxy would have if it were in the field (i.e. without considering the contribution from the cluster). The quoted uncertainty includes contributions from both the data noise and uncertainty on  $\kappa_{\text{ext}}$ . As will be shown in the next section, the small Einstein radius makes SMACS J0723-SL immediately stand out from other previously known strong lenses.

The Sérsic indices of the lens are about 4–5 in all six filters, suggesting that the lens is an early-type galaxy. The half-light radii of the lens are progressively smaller towards redder wavelength, starting from  $\approx 0''.26$  (1.39 kpc) in F090W to  $\approx 0''.19$  (1.02 kpc) in F444W. This trend is consistent with the inside-out growth scenario.

The two components of the source galaxy are separated by  $\approx 0''.09$  (0.761 kpc) in the source plane, and have distinct Sérsic indices (both smaller than  $n = 2$ ). The brighter component, i.e. Component 1, is slightly more compact and less elongated compared to the fainter component. The lensing magnifications for the two components are  $\sim 7.8$  and  $\sim 8.1$ , and they do not vary significantly across the six filters.

#### 4. DISCUSSION

According to our best-fit model, the total enclosed mass of the lens galaxy in SMACS J0723-SL within the iso-density ellipse of semi-major axis  $\theta_E/\sqrt{q_{\text{EPL}}}$  (2.43

kpc) and semi-minor axis  $\sqrt{q_{\text{EPL}}}\theta_E$  (2.11 kpc) is given by

$$M_{\text{lensing}} = \pi\theta_E^2\Sigma_{\text{crit}} = (3.7 \pm 0.2) \times 10^{10} M_{\odot}. \quad (6)$$

To estimate the stellar mass of the lens galaxy, we utilized CIGALE, a public tool designed for fitting the spectral energy distribution (SED) of galaxies (Boquien et al. 2019). We chose the single stellar population (SSP) library from Bruzual & Charlot (2003) and assumed a double exponential star formation history (the `sfh2exp` module). The Salpeter stellar initial mass function (IMF, Salpeter 1955) was employed and the metallicity is fixed to  $Z = 0.02$ . We used the `dustatt_modified_starburst` module, a modification and extension of the Calzetti et al. (2000) attenuation law, for characterizing the dust attenuation. We also included dust emission using the `casey2012` module, which is based on the dust emission model from Casey (2012). We used this model to fit for the observed lens galaxy SED in six NIRCcam filters, and the fitting result is shown in Figure 3. We found a total stellar mass of  $(3.3 \pm 0.8) \times 10^{10} M_{\odot}$ . The projected dark-matter fraction within the half-light radius is thus  $\approx (12 \pm 22)\%$ . We further extracted the spectrum of a  $0''.6 \times 0''.6$  region centered on the lens galaxy from the MUSE data cube and used the pPXF package (Cappellari & Emsellem 2004; Cappellari 2017, 2023) to derive the central stellar velocity dispersion of the lens galaxy. For this analysis, we utilized the E-MILES stellar population synthesis (SPS) models (Vazdekis et al. 2016), which provide UV-extended templates spanning the wavelength range of 1680–50000Å. The fitting result is shown in Figure 3, and the lens galaxy was found to have a velocity dispersion of  $\sigma_* = 140 \pm 6 \text{ km s}^{-1}$ .

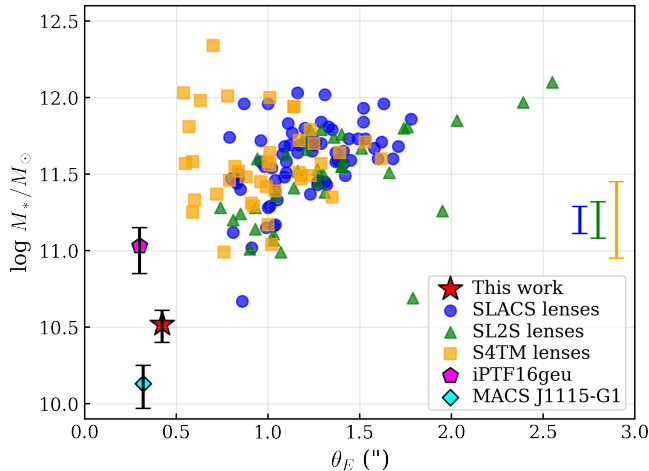


**Figure 4.** Stellar mass versus Einstein radius for a representative subset of known strong lenses. Blue circles represent SLACS lenses, green triangles represent SL2S lenses, orange squares represent S4TM lenses, the magenta pentagon represents iPTF16geu, and the cyan diamond represents MACS J1115-G1. SMACS J0723-SL is indicated by the red star. The blue, green, and orange bars indicate the typical stellar mass uncertainties ( $\pm 1\sigma$ ) for the SLACS, SL2S, and S4TM lenses.

The size, stellar mass, and stellar velocity dispersion measurements all suggest that the lens galaxy in SMACS J0723-SL is indeed a relatively low-mass early-type galaxy. To put into context, we constructed a compilation of previously known strong lenses from the literature. The compilation contains 148 lens galaxies at redshifts  $\approx 0.05 - 0.9$  with published Einstein radius and stellar mass measurements, including 70 from the Sloan Lens ACS Survey (SLACS), 36 from the Strong Lenses in the Legacy Survey (SL2S), 40 from the SLACS for the Masses (S4TM) Survey, iPTF16geu, and another strong lens galaxy discovered in the MACS J1115.9+0129 cluster (i.e. MACS J1115-G1). Although not complete, this compilation is representative of all currently-known galaxy-scale strong lenses in terms of stellar mass and Einstein radius. For the SLACS lenses, Einstein radii and stellar masses were retrieved from Bolton et al. (2008) and Auger et al. (2009). For the SL2S lenses, Einstein radii and stellar masses were retrieved from Sonnenfeld et al. (2013). For the S4TM lenses, Einstein radii and stellar masses were retrieved from Shu et al. (2017). For iPTF16geu, we obtained its Einstein radius from Goobar et al. (2017) and its stellar mass from Arendse et al. (2025). For MACS J1115-G1, Einstein radius and stellar mass were retrieved from Parry et al. (2016). Figure 4 shows the stellar mass-Einstein radius distributions for the known lens

compilation<sup>2</sup> and SMACS J0723-SL. It becomes obvious that the lens galaxy in SMACS J0723-SL is substantially less massive than the majority of known lens galaxies. SMACS J0723-SL thus provides a rare opportunity to peek into a population of galaxies that is largely unexplored in previous strong-lensing studies.

It is worth making a brief comparison between SMACS J0723-SL and MACS J1115-G1, another low-mass strong lens galaxy embedded in a galaxy cluster. According to Parry et al. (2016), MACS J1115-G1 has a similar (lens) redshift of 0.353 and a similarly small Einstein radius of  $0''.32 \pm 0''.04$ . The stellar mass of MACS J1115-G1 is  $(7.6 \pm 2.3) \times 10^9 M_\odot$  assuming a Chabrier IMF (or  $(1.4 \pm 0.4) \times 10^{10} M_\odot$  after converting to a Salpeter IMF), a factor of  $\approx 2.4$  less massive than SMACS J0723-SL. On the other hand, the half-light radius of MACS J1115-G1 is 3.3 kpc, a factor of  $\approx 3$  larger, suggesting that the stellar mass distribution of SMACS J0723-SL appears more compact. The projected dark-matter fraction within the half-light radius is close to 90% for MACS J1115-G1, substantially higher than that of SMACS J0723-SL. More similar measurements will be extremely helpful in characterizing the internal mass structures of galaxies in this mass regime.

SMACS J0723-SL is also a valuable discovery from the perspective of cluster lens modeling. Due to the intrinsic complexity, it is currently infeasible to model all cluster member galaxies in the same detail as is commonly done for galaxy-scale strong lenses. Instead, cluster member galaxies are usually assumed to follow the same mass distribution profile up to a normalization factor, which is determined through an empirical scaling relation (Natarajan & Kneib 1997; Limousin et al. 2007). This conventional modeling approach may introduce significant systematics, especially as there is no consensus on the exact form of the mass profile or scaling relation (Meneghetti et al. 2017). SMACS J0723-SL can provide an exclusive chance of validating the adopted mass profiles and scaling relations by comparing mass models from the conventional approach to those constructed with the strong-lensing features around SMACS J0723-SL taken into account (as achieved in this work). This type of tests will provide important insights into dark matter properties and cosmology which cluster lenses have been used to constrain. For example, Meneghetti

<sup>2</sup> In the original papers, a Chabrier IMF (Chabrier 2003) was assumed in the stellar mass estimations for the S4TM lenses, iPTF16geu, and MACS J1115-G1. To make a more fair comparison, in Figure 4, we added 0.25 dex to their reported stellar masses, which is a typical mass-to-light ratio offset between a Chabrier IMF and a Salpeter IMF for an old stellar population.

et al. (2020) found that observed cluster member galaxies, based on the conventional modeling approach, have noticeably larger lensing cross sections than simulation predictions assuming cold dark matter. They suggested that this discrepancy could arise from the assumption about the nature of dark matter. It would be interesting to verify the estimation of lensing cross sections using systems like SMACS J0723-SL (e.g., Granata et al. 2023).

Although the number of low-mass strong lenses ( $M_* \sim 10^{10.5} M_\odot$ ) is very limited at the moment, ongoing and forthcoming facilities will soon increase the sample size by orders of magnitude. In particular, space missions such as Euclid and China Space Station Telescope (CSST) will be able to discover  $10^5$  galaxy-scale strong lenses with thousands containing low-mass lens galaxies with Einstein radii as small as  $0''.2$  (e.g., Collett 2015; Cao et al. 2024), both in clusters and in fields. With such a large sample, we expect to gain a far more comprehensive understanding of galaxy evolution, the nature of dark matter, and many other aspects.

## 5. CONCLUSION

In summary, we report the discovery of a rare, low-mass strong lens system—SMACS J0723-SL in the SMACS J0723 cluster. MUSE spectroscopic data suggest that the lens and source galaxies are at redshifts of 0.3970 and 1.4792 respectively. By simultaneously modeling JWST NIRCcam imaging data in six filters, i.e. F090W, F150W, F200W, F277W, F356W, and F444W, we find that the Einstein radius of the lens galaxy in SMACS J0723-SL is  $0''.424 \pm 0''.012$ , which corresponds

to a total enclosed mass of  $(3.7 \pm 0.2) \times 10^{10} M_\odot$ . The half-light radius of the lens galaxy decreases from  $0''.2604$  (1.39 kpc) in the F090W to  $0''.1935$  (1.02 kpc) in F444W, and the central velocity dispersion is found to be  $140 \pm 6$  km s $^{-1}$ . The stellar mass of the lens galaxy is estimated to be  $(3.3 \pm 0.8) \times 10^{10} M_\odot$  from fitting the photometry in six JWST filters. The dark-matter fraction within the half-light radius is  $\approx (12 \pm 22)\%$ .

SMACS J0723-SL is one of the few known cases that contains a low-mass lens galaxy of  $M_* \sim 10^{10.5} M_\odot$ , which is about an order of magnitude lower than the average mass of all galaxy-scale strong lenses discovered to date. It hence presents a rare opportunity to investigate a population of galaxies that has remained largely unexplored in previous strong-lensing studies. In the near future, thousands of low-mass strong lenses with Einstein radii as small as  $0''.2$  will be discovered by missions such as Euclid and CSST, which will provide further constraints on galaxy evolution, dark matter, and cosmology.

We would like to thank the anonymous referee for their helpful comments, which improved the presentation of this work. This work is supported by the National Key R&D Program of China (grant No. 2023YFA1608100).

*Facilities:* JWST, MUSE

*Software:* lenstronomy (Birrer & Amara 2018), pPXF (Cappellari & Emsellem 2004; Cappellari 2017, 2023), CIGALE (Boquien et al. 2019)

## REFERENCES

- Arendse, N., Mörtzell, E., Weisenbach, L., et al. 2025, arXiv e-prints, arXiv:2501.01578, doi: [10.48550/arXiv.2501.01578](https://doi.org/10.48550/arXiv.2501.01578)
- Auger, M. W., Treu, T., Bolton, A. S., et al. 2009, ApJ, 705, 1099, doi: [10.1088/0004-637X/705/2/1099](https://doi.org/10.1088/0004-637X/705/2/1099)
- . 2010, ApJ, 724, 511, doi: [10.1088/0004-637X/724/1/511](https://doi.org/10.1088/0004-637X/724/1/511)
- Birrer, S., & Amara, A. 2018, Physics of the Dark Universe, 22, 189, doi: [10.1016/j.dark.2018.11.002](https://doi.org/10.1016/j.dark.2018.11.002)
- Bolton, A. S., Burles, S., Koopmans, L. V. E., et al. 2008, ApJ, 682, 964, doi: [10.1086/589327](https://doi.org/10.1086/589327)
- Bolton, A. S., Brownstein, J. R., Kochanek, C. S., et al. 2012, ApJ, 757, 82, doi: [10.1088/0004-637X/757/1/82](https://doi.org/10.1088/0004-637X/757/1/82)
- Boquien, M., Burgarella, D., Roehlly, Y., et al. 2019, A&A, 622, A103, doi: [10.1051/0004-6361/201834156](https://doi.org/10.1051/0004-6361/201834156)
- Bruderer, C., Read, J. I., Coles, J. P., et al. 2016, MNRAS, 456, 870, doi: [10.1093/mnras/stv2582](https://doi.org/10.1093/mnras/stv2582)
- Bruzual, G., & Charlot, S. 2003, MNRAS, 344, 1000, doi: [10.1046/j.1365-8711.2003.06897.x](https://doi.org/10.1046/j.1365-8711.2003.06897.x)
- Calzetti, D., Armus, L., Bohlin, R. C., et al. 2000, ApJ, 533, 682, doi: [10.1086/308692](https://doi.org/10.1086/308692)
- Caminha, G. B., Suyu, S. H., Mercurio, A., et al. 2022, A&A, 666, L9, doi: [10.1051/0004-6361/202244517](https://doi.org/10.1051/0004-6361/202244517)
- Cao, X., Li, R., Li, N., et al. 2024, MNRAS, 533, 1960, doi: [10.1093/mnras/stae1865](https://doi.org/10.1093/mnras/stae1865)
- Cappellari, M. 2017, MNRAS, 466, 798, doi: [10.1093/mnras/stw3020](https://doi.org/10.1093/mnras/stw3020)
- . 2023, MNRAS, 526, 3273, doi: [10.1093/mnras/stad2597](https://doi.org/10.1093/mnras/stad2597)
- Cappellari, M., & Emsellem, E. 2004, PASP, 116, 138, doi: [10.1086/381875](https://doi.org/10.1086/381875)
- Cappellari, M., Scott, N., Alatalo, K., et al. 2013a, MNRAS, 432, 1709, doi: [10.1093/mnras/stt562](https://doi.org/10.1093/mnras/stt562)



- Cappellari, M., McDermid, R. M., Alatalo, K., et al. 2013b, *MNRAS*, 432, 1862, doi: [10.1093/mnras/stt644](https://doi.org/10.1093/mnras/stt644)
- Casey, C. M. 2012, *MNRAS*, 425, 3094, doi: [10.1111/j.1365-2966.2012.21455.x](https://doi.org/10.1111/j.1365-2966.2012.21455.x)
- Chabrier, G. 2003, *PASP*, 115, 763, doi: [10.1086/376392](https://doi.org/10.1086/376392)
- Collett, T. E. 2015, *ApJ*, 811, 20, doi: [10.1088/0004-637X/811/1/20](https://doi.org/10.1088/0004-637X/811/1/20)
- Falco, E. E., Gorenstein, M. V., & Shapiro, I. I. 1985, *ApJL*, 289, L1, doi: [10.1086/184422](https://doi.org/10.1086/184422)
- Golubchik, M., Furtak, L. J., Meena, A. K., & Zitrin, A. 2022, *ApJ*, 938, 14, doi: [10.3847/1538-4357/ac8ff1](https://doi.org/10.3847/1538-4357/ac8ff1)
- Goobar, A., Amanullah, R., Kulkarni, S. R., et al. 2017, *Science*, 356, 291, doi: [10.1126/science.aal2729](https://doi.org/10.1126/science.aal2729)
- Granata, G., Bergamini, P., Grillo, C., et al. 2023, *A&A*, 679, A124, doi: [10.1051/0004-6361/202347521](https://doi.org/10.1051/0004-6361/202347521)
- Khadka, N., Birrer, S., Leauthaud, A., & Nix, H. 2024, *MNRAS*, 533, 795, doi: [10.1093/mnras/stae1832](https://doi.org/10.1093/mnras/stae1832)
- Koopmans, L. V. E., Treu, T., Bolton, A. S., Burles, S., & Moustakas, L. A. 2006, *ApJ*, 649, 599, doi: [10.1086/505696](https://doi.org/10.1086/505696)
- Li, H., Ge, J., Mao, S., et al. 2017, *ApJ*, 838, 77, doi: [10.3847/1538-4357/aa662a](https://doi.org/10.3847/1538-4357/aa662a)
- Li, R., Shu, Y., & Wang, J. 2018, *MNRAS*, 480, 431, doi: [10.1093/mnras/sty1813](https://doi.org/10.1093/mnras/sty1813)
- Limousin, M., Richard, J., Jullo, E., et al. 2007, *ApJ*, 668, 643, doi: [10.1086/521293](https://doi.org/10.1086/521293)
- Mahler, G., Jauzac, M., Richard, J., et al. 2023, *ApJ*, 945, 49, doi: [10.3847/1538-4357/acaea9](https://doi.org/10.3847/1538-4357/acaea9)
- Meneghetti, M., Natarajan, P., Coe, D., et al. 2017, *MNRAS*, 472, 3177, doi: [10.1093/mnras/stx2064](https://doi.org/10.1093/mnras/stx2064)
- Meneghetti, M., Davoli, G., Bergamini, P., et al. 2020, *Science*, 369, 1347, doi: [10.1126/science.aax5164](https://doi.org/10.1126/science.aax5164)
- Natarajan, P., & Kneib, J.-P. 1997, *MNRAS*, 287, 833, doi: [10.1093/mnras/287.4.833](https://doi.org/10.1093/mnras/287.4.833)
- Nie, L., Shan, H., Li, G., et al. 2023, arXiv e-prints, arXiv:2308.14065, doi: [10.48550/arXiv.2308.14065](https://doi.org/10.48550/arXiv.2308.14065)
- Nipoti, C., Treu, T., & Bolton, A. S. 2009, *ApJ*, 703, 1531, doi: [10.1088/0004-637X/703/2/1531](https://doi.org/10.1088/0004-637X/703/2/1531)
- Oguri, M., Rusu, C. E., & Falco, E. E. 2014, *MNRAS*, 439, 2494, doi: [10.1093/mnras/stu106](https://doi.org/10.1093/mnras/stu106)
- Parry, W. G., Grillo, C., Mercurio, A., et al. 2016, *MNRAS*, 458, 1493, doi: [10.1093/mnras/stw298](https://doi.org/10.1093/mnras/stw298)
- Pontoppidan, K. M., Barrientes, J., Blome, C., et al. 2022, *ApJL*, 936, L14, doi: [10.3847/2041-8213/ac8a4e](https://doi.org/10.3847/2041-8213/ac8a4e)
- Salpeter, E. E. 1955, *ApJ*, 121, 161, doi: [10.1086/145971](https://doi.org/10.1086/145971)
- Schneider, P., & Sluse, D. 2013, *A&A*, 559, A37, doi: [10.1051/0004-6361/201321882](https://doi.org/10.1051/0004-6361/201321882)
- Sérsic, J. L. 1963, *Boletín de la Asociación Argentina de Astronomía La Plata Argentina*, 6, 41
- Shajib, A. J., Treu, T., Birrer, S., & Sonnenfeld, A. 2021, *MNRAS*, 503, 2380, doi: [10.1093/mnras/stab536](https://doi.org/10.1093/mnras/stab536)
- Sharon, K., Chen, M. C., Mahler, G., Coe, D., & RELICS: Reionization Lensing Cluster Survey. 2023, *ApJS*, 264, 15, doi: [10.3847/1538-4365/aca7c3](https://doi.org/10.3847/1538-4365/aca7c3)
- Shu, Y., Bolton, A. S., Brownstein, J. R., et al. 2015, *ApJ*, 803, 71, doi: [10.1088/0004-637X/803/2/71](https://doi.org/10.1088/0004-637X/803/2/71)
- Shu, Y., Bolton, A. S., Mao, S., et al. 2016, *ApJ*, 833, 264, doi: [10.3847/1538-4357/833/2/264](https://doi.org/10.3847/1538-4357/833/2/264)
- Shu, Y., Brownstein, J. R., Bolton, A. S., et al. 2017, *ApJ*, 851, 48, doi: [10.3847/1538-4357/aa9794](https://doi.org/10.3847/1538-4357/aa9794)
- Sonnenfeld, A., Gavazzi, R., Suyu, S. H., Treu, T., & Marshall, P. J. 2013, *ApJ*, 777, 97, doi: [10.1088/0004-637X/777/2/97](https://doi.org/10.1088/0004-637X/777/2/97)
- Sonnenfeld, A., Nipoti, C., & Treu, T. 2014, *ApJ*, 786, 89, doi: [10.1088/0004-637X/786/2/89](https://doi.org/10.1088/0004-637X/786/2/89)
- Spiniello, C., Koopmans, L. V. E., Trager, S. C., Czoske, O., & Treu, T. 2011, *MNRAS*, 417, 3000, doi: [10.1111/j.1365-2966.2011.19458.x](https://doi.org/10.1111/j.1365-2966.2011.19458.x)
- Vazdekis, A., Koleva, M., Ricciardelli, E., Röck, B., & Falcón-Barroso, J. 2016, *MNRAS*, 463, 3409, doi: [10.1093/mnras/stw2231](https://doi.org/10.1093/mnras/stw2231)
- Velliscig, M., van Daalen, M. P., Schaye, J., et al. 2014, *MNRAS*, 442, 2641, doi: [10.1093/mnras/stu1044](https://doi.org/10.1093/mnras/stu1044)
- Wang, L., Li, G., & Kang, X. 2022, *MNRAS*, 517, 787, doi: [10.1093/mnras/stac2664](https://doi.org/10.1093/mnras/stac2664)
- Wang, L., Shan, H., Nie, L., et al. 2025, *ApJS*, 276, 36, doi: [10.3847/1538-4365/ad9566](https://doi.org/10.3847/1538-4365/ad9566)